12-16-2019

In-Plane Vibration of Hammerhead Resonators for Chemical Sensing Applications

Luke A. Beardslee
Georgia Institute of Technology - Main Campus

Christopher Carron
Georgia Institute of Technology - Main Campus

Kemal S. Demirci
Georgia Institute of Technology - Main Campus

Jonathan Lehman
Georgia Institute of Technology

Steven Schwartz
Georgia Institute of Technology

See next page for additional authors

ACS Sensors, Vol. 5, No. 1 (December 16, 2019): 73-82. DOI.

In-Plane Vibration of Hammerhead Resonators for Chemical Sensing Applications

Luke A. Beardslee
School of Electrical and Computer Engineering, Georgia Institute of Technology, Atlanta, Georgia
Naval Submarine Medical Research Laboratory, Groton, Connecticut
Christopher Carron
School of Electrical and Computer Engineering, Georgia Institute of Technology, Atlanta, Georgia
Space and Intelligence Systems, Harris Corporation, Melbourne, Florida
Kemal S. Demirci
School of Electrical and Computer Engineering, Georgia Institute of Technology, Atlanta, Georgia
Texas Instruments, Inc., Dallas, Texas
Jonathan Lehman
School of Electrical and Computer Engineering, Georgia Institute of Technology, Atlanta, Georgia
Steven Schwartz
School of Electrical and Computer Engineering, School of Material Science and Engineering, Institute for Electronics and Nanotechnology, Georgia Institute of Technology, Atlanta, Georgia
Isabelle Dufour

IMS Laboratory, University of Bordeaux, Talence 33400, France
Stephen M. Heinrich
Department of Civil, Construction and Environmental Engineering, Marquette University, Milwaukee, Wisconsin
Fabien Josse
Department of Electrical and Computer Engineering, Marquette University, Milwaukee, Wisconsin
Oliver Brand
School of Electrical and Computer Engineering, Institute for Electronics and Nanotechnology, Georgia Institute of Technology, Atlanta, Georgia

Abstract

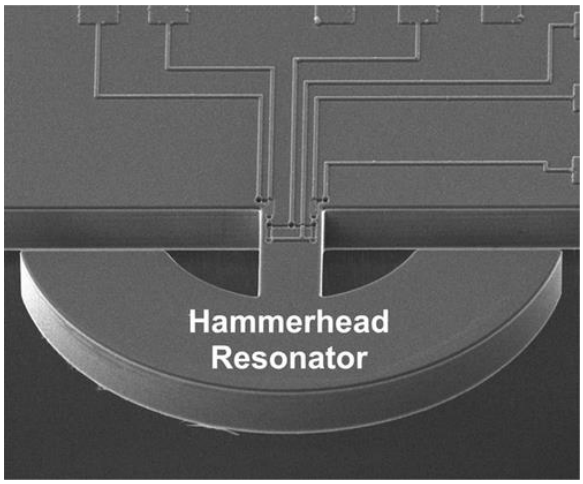

Thermally excited and piezoresistively detected in-plane cantilever resonators have been previously demonstrated for gas- and liquid-phase chemical and biosensing applications. In this work, the hammerhead resonator geometry, consisting of a cantilever beam supporting a wider semicircular “head”, vibrating in an in-plane vibration mode, is shown to be particularly effective for gas-phase sensing with estimated limits of detection in the sub-ppm range for volatile organic compounds. This paper discusses the hammerhead resonator design and the particular advantages of the hammerhead geometry, while also presenting mechanical characterization, optical characterization, and chemical sensing results. These data highlight the distinct advantages of the hammerhead geometry over other cantilever designs.

KEYWORDS:

chemical sensor, volatile organic compounds, cantilever, resonator, in-plane flexural mode

For many real-world chemical sensing applications, including environmental monitoring, occupational exposure monitoring, threat detection, and medical applications, the gold standard method is to collect samples in the field and then to send them to an analytical lab for analysis using gas chromatography and mass spectrometry (GC–MS). While these analytical methods are selective and highly sensitive, they are expensive, time-consuming, and do not provide results in real time. However,

the application areas outlined above could all potentially benefit from sensors or networks of sensors that provide real-time data to their users. For such applications, batch-fabricated microsensors based on microelectromechanical system (MEMS) technologies are appealing because these sensors can be fabricated inexpensively in large numbers, often using technologies adopted from integrated circuit fabrication. To this end, a wide variety of chemical microsensors using different transduction mechanisms, including electrochemical, optical, thermal, and mechanical sensors, have been demonstrated, each with their unique advantages and challenges.(1−6) Generally, these chemical microsensors have not (yet) demonstrated the sensitivity, stability, and particularly selectivity achieved with laboratory-based GC–MS equipment. They do, however, offer small size, low cost, in-field usability, and real-time data, all of which are key requirements for many (novel) sensing scenarios.

One class of such miniaturized chemical sensors are mass-sensitive microsensors based on mechanical resonators coated with an appropriate sensing film.(7−13) Mass-sensitive chemical sensors benefit from the relative simplicity of their excitation and detection methods, as well as the additional advantage that mass detection is a well-characterized parameter. As with chemical sensors in general, a wide variety of mass-sensitive sensor designs have been demonstrated ranging from acoustic wave devices(14−16) to micromachined resonators, such as cantilever beams.(7,8,10,12,13,17,18) The various designs have employed a wide range of excitation and detection schemes, including electrostatic, piezoelectric, and thermal excitation, as well as capacitive, piezoelectric, piezoresistive, and optical detection. While many of the devices are based on silicon or related materials, such as SiO_2 and SiN_x, alternative materials including polymers, such as SU-8,(12,19) and more recently diamond(20,21) have been investigated for chemical sensing applications. While polymer-based cantilever sensors benefit from inexpensive, low-temperature fabrication, they are predominantly operated in a static bending mode rather than a dynamic, resonant mode because of the inherent viscoelastic damping of the polymers themselves.(19)

For the micromachined, resonant devices, the underlying physics is well-understood, where the added mass upon sorption of the analyte of interest lowers the resonance frequency of a particular vibration mode of the mechanical resonator. In the case of acoustic wave devices, typically operated in a two port configuration within an oscillating feedback loop, the mass added to the surface results in a change in the acoustic wave velocity and attenuation, altering the resonant frequency of the oscillator circuit.(14−16) Around a particular resonance frequency, the resonator itself is typically modeled, at least to a first order, using the differential equation for a second-order mass-spring-damper system. The resulting frequency change upon mass loading can be read easily with appropriate readout circuitry.

Cantilever-based resonant chemical sensors have been of particular interest because of their simple design, ease of fabrication, and potential for high sensitivity.(7,8,9,10,12,13,17) Traditionally, cantilever-based resonant chemical sensors have been operated using out-of-plane (OOP) flexural modes (similar to diving boards), but more recent work highlights the benefits of operating them in in-plane (IP) flexural modes, thereby reducing the damping and the shift in resonance frequency because of the added fluid mass when immersed in fluids, particularly liquids.(22−25)

This paper focuses on the performance of cantilever-based resonant chemical sensors operated in their fundamental IP flexural vibration mode, with a particular emphasis on the use of so-called

hammerhead resonators, consisting of a suspended platform (coated with the sensing film) which is supported by a cantilever beam. Figure 1 compares the mode shapes, obtained using finite element modeling (FEM), of a prismatic cantilever beam operated in the first OOP mode and the first IP mode, as well as a hammerhead resonator with a semiannular end platform operated in its first IP mode, illustrating the differences in device geometry and operation mode shape. The color coding represents the dominating stress in *x*-direction, which is primarily explored to selectively sense the IP vibration mode while rejecting signals from undesired OOP and torsional modes. A detailed description of how the IP mode is excited and preferentially sensed using piezo-resistors in a Wheatstone bridge can be found elsewhere.(24)

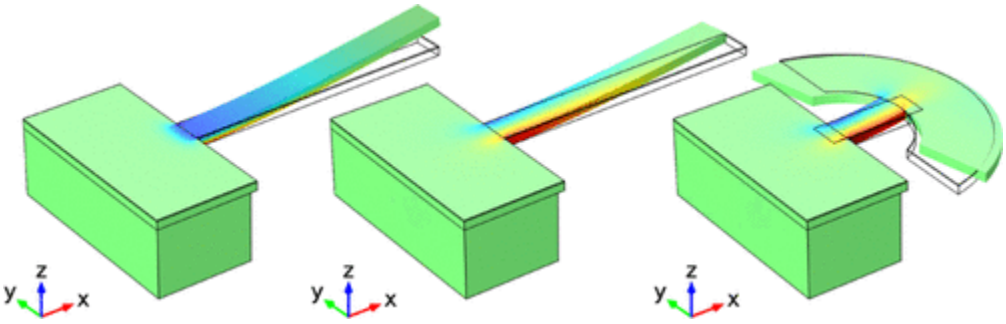

Figure 1. FEM simulation of the (left) fundamental OOP (first OOP) and (center) fundamental IP (first IP) vibration mode of a 400 µm long, 45 µm wide silicon cantilever, as well as the (right) fundamental IP (first IP) vibration mode of a hammerhead resonator with a semicircular annulus having an outer radius of 200 µm and a 45 µm wide, 100 µm long stem. The colors correspond to the *x*-directed stress in the microresonators as they deflect.

The following sections discuss the hammerhead resonator design and fabrication, the theory of operation of IP mode cantilevers, the specific advantages of the hammerhead structures, the characterization of the hammerhead devices, and their application as gas-phase chemical sensors.

Design and Fabrication

The hammerhead resonators comprise a semicircular head region, which is supported by a cantilever stem. Figure 2 illustrates two different designs investigated in this work, together with the fundamental design parameter values and ranges. For equal *L*, *b*, *R*, and device thickness *h*, both designs have similar resonance frequencies and Q-factors, particularly for the fundamental IP vibration mode of interest to this work. However, design A with inner radius *r* generally led to better chemical sensing performance; it is believed that the small gap *s* of design B tends to clog with polymeric sensing film during film deposition, which lowers the Q -factor and sensing performance of the coated resonators for this design.

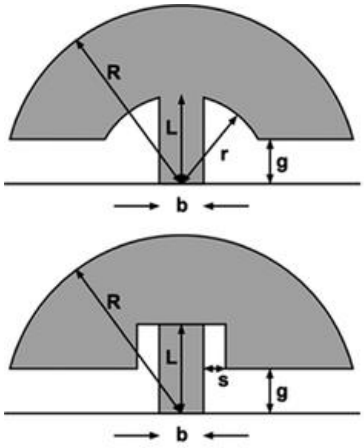

Design A: F150A, F200A

Stem Length: L = 100 μm
Stem Width: b = 45 μm
Gap: g = 45 μm
Outer Radius: R = 150, 200 μm
Inner Radius: r = 100 μm

Design B: F150B, F200B

Stem Length: L = 100 μm
Stem Width: b = 45 μm
Gap: g = 45 μm
Small Gap: s = 10 μm
Outer Radius: R = 150, 200 μm

Figure 2. Layout of two design variants (design A and design B) of the hammerhead resonator with a semicircular annulus with device dimensions. The designations F200A and F200B refer to a hammerhead resonator with *R* = 200 μm outer radius with letters A and B referring to designs A and B, respectively. Similarly, F150A and F150B refer to a hammerhead with *R* = 150 μm in designs A and B, respectively.

Finite element simulation was employed to estimate the frequencies of the different vibration modes of the hammerhead structures. As an example, Figure 3a,b shows the dependence of the four lowest vibration modes of the design-A-based resonator with 200 μm outer radius (F200A) on the width of the cantilever stem *b* and the silicon thickness *h*, respectively. As expected, the frequency of the fundamental IP vibration mode strongly depends on the stem width but is almost independent of the silicon thickness, whereas the frequencies of the OOP and torsional modes strongly depend on the silicon thickness but are less affected by the stem width. In general, device dimensions were chosen for which the fundamental IP vibration mode (first IP) is not overlapping or adjacent to other modes, so as to maintain its high Q -factor and simplify closed-loop operation of the resonators.

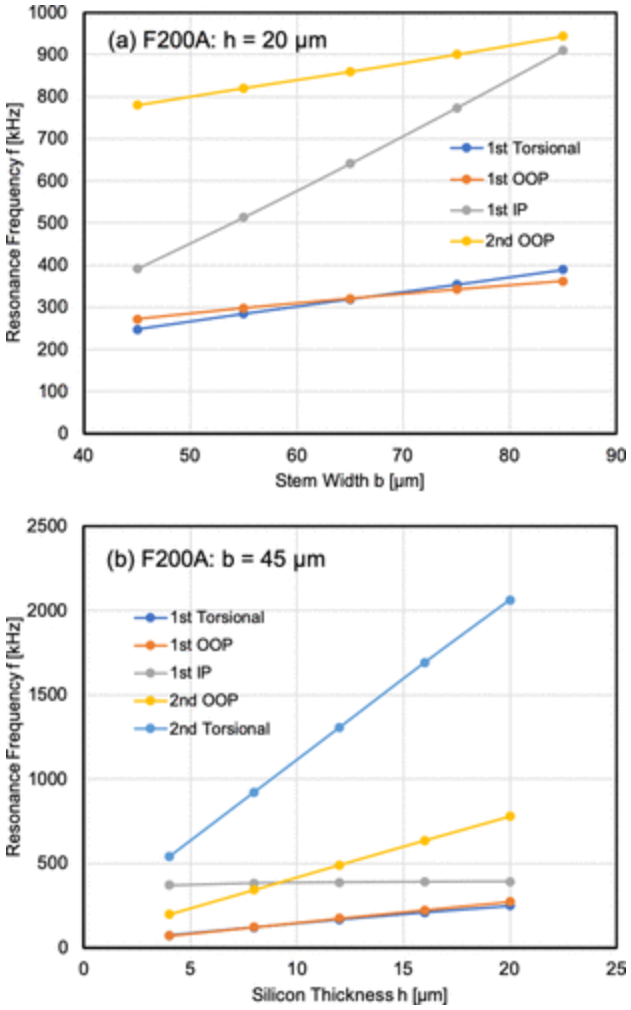

Figure 3. Simulated (vacuum) resonance frequencies of first and second OOP, first IP, as well as first and second torsional modes of hammerhead resonator F200A (design A, *R* = 200 µm) as a function of (a) stem width *b* (for a silicon thickness of 20 µm) and (b) silicon thickness *h* (for a stem width of 45 µm). The simulated resonators were passivated using a 2 µm-thick silicon dioxide passivation layer. No sensing film was added in the simulation.

Thermal actuation and piezoresistive detection were chosen for exciting and sensing the first IP flexural mode of the hammerhead resonators. Thermal actuation and piezoresistive detection both rely on resistors as transduction elements, which are straightforward to integrate with the utilized silicon-based bulk micromachining process. In order to reject common mode signals and also possible signals from unwanted modes, the piezoresistors are arranged in a Wheatstone bridge configuration. Thereby, a U-shaped Wheatstone bridge (see Supporting Information, Figure S1) promotes signals stemming from the desired IP vibration mode, but—to first order—rejects signals from OOP and torsional modes because of the resistor arrangement and characteristic stress distribution of the different modes. This particular resistor layout is discussed in detail elsewhere.(24) Promotion of the IP mode over other undesired flexural modes is essential for the proper operation of the hammerhead resonators in an amplifying feedback loop. For device excitation in the IP vibration mode, one of the two heating resistors located in the high stress region near the clamped edge of the cantilever is driven with an ac voltage superimposed on a dc voltage to prevent frequency doubling.

Figure S2 in the Supporting Information outlines the basic complementary metal oxide semiconductor (CMOS) compatible fabrication process used to manufacture the hammerhead resonators. The basic process flow, which has been described in detail earlier,(26) can be modified to use silicon on insulator wafers and to accommodate thicker or thinner passivation layers depending on whether the hammerheads (or cantilevers) will be operated in air or water. Figure 4 shows a scanning electron microscopy (SEM) image of a fabricated device.

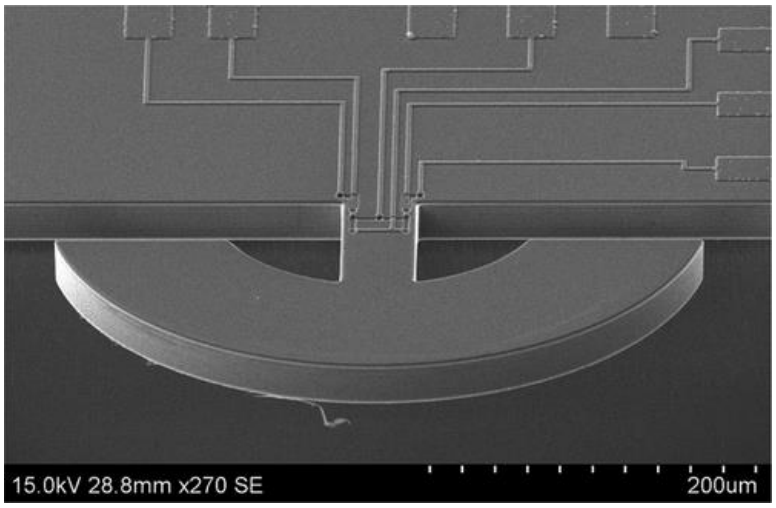

Figure 4. SEM micrograph of a F200A hammerhead device with a 45 µm wide and 100 µm long support cantilever and a semicircular annulus with an outer radius of 200 µm. The piezoresistive Wheatstone bridge and thermal excitation resistors can be seen at the base of the device.

Theory of IP Mode Cantilevers

A key performance metric for any (bio)chemical sensor is its limit of detection (LOD), that is, the smallest detectable concentration of analyte in the surrounding medium. In the case of a resonant (mass-sensitive) chemical sensor, the LOD (in ppm) is generally defined as 3 times the noise-equivalent analyte concentration, which itself is given by the ratio of the short-term frequency fluctuation, $\Delta f_{\min}$ (in Hz), determined, for example, via the Allan variance method,(27) and the chemical sensor sensitivity *S* (in Hz/ppm)

$$\mathrm{LOD} = 3\frac{\Delta f_{\min}}{S} \quad (1)$$

The LOD can also be expressed as 3 times the ratio of the relative short-term frequency fluctuation $\sigma_{\min}$ to the relative chemical sensor sensitivity S_R

$$\mathrm{LOD} = 3\frac{\sigma_{\min}}{S_{\mathrm{R}}} = 3\frac{\Delta f_{\min}/f}{S/f} \quad (2)$$

As described in refs,(23,28) the chemical sensitivity *S* (or relative chemical sensitivity S_R) may be written as the product of the gravimetric sensitivity *G* (or the relative gravimetric sensitivity G_R) of the coated resonant sensor, that is, the absolute or relative change in frequency f because of a change in density ρ_m of the sensing film, and the analyte sensitivity S_A, that is, the change in the sensing film density ρ_m because of a change in analyte concentration c_A in the surrounding medium

$$S = GS_A = \frac{\partial f}{\partial p_m}\frac{\partial p_m}{\partial c_A} \quad (3)$$

$$S_R = G_R S_A = \left[\frac{1}{f}\frac{\partial f}{\partial p_m}\right]\frac{\partial p_m}{\partial c_A} \quad (4)$$

From eqs 1–4, the sensor LOD can be improved by increasing the (relative) gravimetric sensitivity *G* or G_R, increasing the analyte sensitivity S_A, or improving the (relative) frequency stability, that is, reducing $\Delta f_{\min}$ or $\sigma_{\min}$. The analyte sensitivity S_A can be optimized for a given analyte by proper choice of the sensing film and is not the focus of this work. In the following, the dependence of the relative gravimetric sensitivity G_R and the short-term frequency fluctuation $\Delta f_{\min}$ ($\sigma_{\min}$) on the device geometry will be analyzed in detail for the case of prismatic cantilevers and then generalized to include hammerhead resonators.

If we assume a prismatic cantilever (see the Supporting Information, Figure S3) with length *L*, width *b*, and thickness *h*, clamped along the *x* = 0 plane, the frequencies of the IP (i.e., deflection in *y*-direction) flexural modes in vacuum (in units of rad/s) are given by(29)

$$\omega_i = \frac{\lambda_i^2}{\sqrt{12}}\frac{b}{L^2}\sqrt{\frac{E_{\mathrm{eff}}}{\rho_{\mathrm{eff}}}} \quad (5)$$

as long as $L \gg b$, that is, the conditions for the validity of elementary beam theory are fulfilled. λ_i is the mode factor for mode *i* (with $\lambda_1 = 1.8751$ for the fundamental mode), while E_{eff} and ρ_{eff} represent the effective Young's modulus and density of the cantilever, respectively. Assuming that only the effective density of the cantilever is changed by analyte sorption into the sensing film, the relative frequency change per change in analyte concentration Δc_{A} can simply be approximated as

$$\frac{1}{\omega_i}\frac{\Delta\omega_i}{\Delta c_A} = \frac{1}{f_i}\frac{\Delta f_i}{\Delta c_A} = \frac{1}{\omega_i}\frac{\mathrm{d}\omega_i}{\mathrm{d}\rho_{\mathrm{eff}}}\frac{\mathrm{d}\rho_{\mathrm{eff}}}{\mathrm{d}c_A} = \frac{1}{2}\frac{1}{\rho_{\mathrm{eff}}}\frac{\mathrm{d}\rho_{\mathrm{eff}}}{\mathrm{d}c_A} \quad (6)$$

For higher analyte concentrations, the above assumption may no longer be valid, and the analyte sorption may also affect the Young's modulus.(30) However, this additional effect does not change the conclusions drawn in the following. Notably, eq 6 is independent of the dimensions of the cantilever. Assuming that the cantilever has a uniform layered structure, with the top layer (*m*-th layer) being the sensing film, the effective film density can be written as the weighted average of the densities of the different layers

$$\rho_{\mathrm{eff}} = \frac{1}{h}\left[\sum_{n=1}^{m} h_n\rho_n + h_m S_A c_A\right] \quad (7)$$

where h_n and ρ_n are the thickness and density of the *n*-th layer and the last term describes the (weighted) added density of the *m*-th layer (sensing film) because of the sorbed analyte. Using eqs 6 and 7, it can be easily shown that, for small density changes upon analyte loading, the relative chemical and gravimetric sensitivities S_R and G_R become

$$S_R = \frac{1}{f}\frac{\Delta f}{\Delta c_A} = -\frac{1}{2}\frac{1}{\rho_{\mathrm{eff}}}\frac{\mathrm{d}\rho_{\mathrm{eff}}}{\mathrm{d}c_A} = -\frac{1}{2}\frac{h_m S_A}{h_{\rho_{\mathrm{eff}}}} \approx -\frac{1}{2}\frac{h_m S_A}{\sum_{n=1}^{m} h_n\rho_n} \quad (8)$$

$$G_R\frac{1}{f}\frac{\Delta f}{\Delta\rho_m} = -\frac{1}{2}\frac{1}{\rho_{\mathrm{eff}}}\frac{\mathrm{d}\rho_{\mathrm{eff}}}{\mathrm{d}\rho_m} = -\frac{1}{2}\frac{h_m}{h_{\rho_{\mathrm{eff}}}} \approx -\frac{1}{2}\frac{h_m}{\sum_{n=1}^{m} h_n\rho_n} \quad (9)$$

Thus, the relative chemical and gravimetric sensitivities S_R and G_R do not depend on the IP dimensions (length or width) of the cantilever but only on the thicknesses of the films of the layered structure. While eqs 8 and 9 were derived for a prismatic cantilever with a uniform layered structure using eq 5, the results can be generalized for flexural modes where the resonance frequency is proportional to $\sqrt{E_{\text{eff}}/\rho_{\text{eff}}}$. Thus, the results shown in eqs 8 and 9 are not only valid for IP resonance modes but also for OOP modes and, more importantly for this work, are not limited to prismatic beams but apply to any beam geometry, including the hammerhead resonators discussed in this work. Again, the underlying assumptions are (i) the conditions for elementary beam theory apply, (ii) a uniform layered structure of the resonator (including the sensing film) throughout the entire device (beam and hammerhead platform), and (iii) the fact that the analyte sorption affects only the sensing film density, but not its geometry or stiffness. It should be noted that—in the case of the hammerhead resonators—it may be desirable to coat only the head region (not the stem) with sensing film in order to minimize the Q -factor degradation (because of the viscoelastic damping from the polymer film); in this case, the Q enhancement will be accompanied by a small reduction in the values of S_R and G_R as given by eqs 8 and 9, that is, these equations provide upper bounds on the relative sensitivities.

To verify eq 9, the FEM software COMSOL (Stockholm, Sweden) has been used to simulate the gravimetric sensitivity of cantilever and hammerhead resonators with a uniform layer structure, while varying IP dimensions (L = 200–800 µm and b = 45–90 µm in the case of cantilevers) and, thus, resonance frequencies. In the simulations, the (relative) change in resonance frequency due to a density change in the sensing film was extracted from two modal analyses performed with two sensing film densities, using the same mesh for both analyses. Figure 1 shows typical finite element models, with part of the silicon–support structure being modeled to account for the nonideal clamping of the cantilever. Figure 5 summarizes the absolute values of the simulated relative gravimetric sensitivities of the various resonators with the same layer structure as a function of the resonance frequency. For the layer sandwich chosen [10 µm Si, 2 µm SiO_2 passivation, and a 3 µm-thick polydimethylsiloxane (PDMS) sensing film], the relative gravimetric sensitivity calculated using eq 9 is $G_R = -4.9 \times 10^{-5}$ m³/kg, which agrees well with the simulated values at frequencies below 200 kHz (see Figure 5). As expected from eq 9 and the earlier discussion, the G_R simulated for the OOP modes of cantilever and hammerhead resonators with frequencies ranging from approximately 20 kHz to 1 MHz remain within 10% of the expected value. However, the simulated G_R for the fundamental IP mode increases more rapidly for both prismatic cantilevers and hammerhead resonators, exceeding 10% increase for frequencies >300 kHz. It is believed that the non-negligible shear deformation, in particular in the first IP mode for devices with small L/b ratios, that is, high-resonance frequencies, is responsible for this deviation from eq 9; as mentioned before, eq 9 is based on eq 5, which assumes a large L/b value. It is also worth noting that the simulated gravimetric sensitivity only marginally decreases for hammerhead resonators where only the head region is coated: for F200A and F150A resonators with a 45 µm-wide and 100 µm-long stem, the absolute value of G_R for the first IP mode decreases by only 1.6% (from 5.57×10^{-5} to 5.48×10^{-5} m³/kg) and 2.3% (from 8.54×10^{-5} to 8.34×10^{-5} m³/kg), respectively, when coating only the head region versus the full resonator surface.

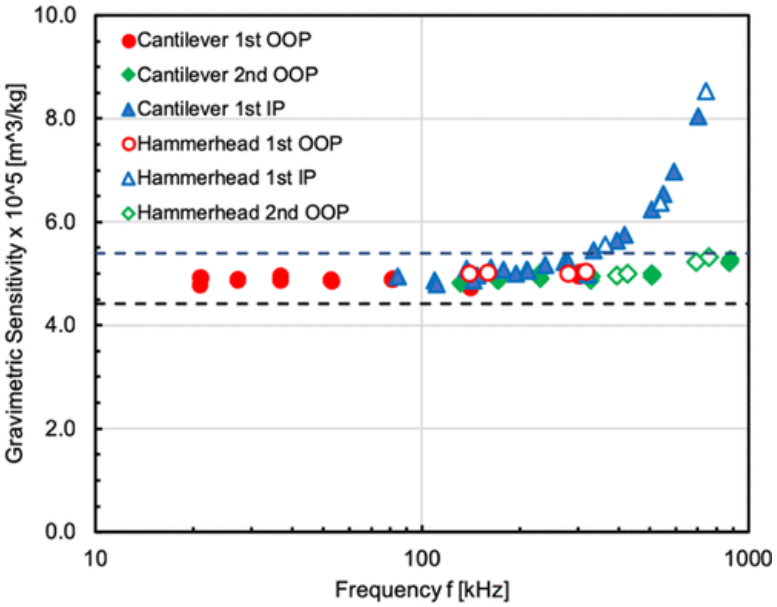

Figure 5. Simulated absolute value of the relative gravimetric sensitivity as a function of resonance frequency for prismatic cantilevers (solid symbols) and hammerhead resonators (open symbols) with varying lateral dimensions (L = 200–800 µm and b = 45–90 µm for the cantilevers), but the same layer sandwich (10 µm Si, 2 µm SiO_2, and a 3 µm PDMS sensing film). Data shown are for the fundamental OOP mode (circles), the second OOP mode (diamonds), and the fundamental IP mode (triangles). The dashed lines represent ±10% boundaries from the theoretical value of $|G_R|$ = 4.9 × 10^{-5} m^3/kg.

If the IP beam dimensions and the flexural mode of interest do not affect the relative gravimetric sensitivity, how can the designer improve the sensor LOD? The answer is twofold: first, the relative gravimetric sensitivity can be increased by optimizing the layer sandwich (see eq 9), that is, by increasing h_m and/or reducing the denominator $\sum_{n=1}^{m} h_n \rho_n$. The extreme case would be a resonator only comprising the sensing film, in which case, the gravimetric sensitivity simply becomes $G_R = -1/2\rho_m$, that is, it is inversely proportional to the sensing film density. This limit may practically be difficult to achieve, as the sensing films generally need a support structure with integrated excitation and detection elements (though it has been accomplished(31)). However, minimizing the thickness of nonsorbing materials with respect to the thickness of the sensing film is generally advised. In doing so, caution must be exercised not to degrade the frequency stability of the resonator while optimizing the layer sandwich, as will be discussed in the following. According to eq 2, the second way to optimize the LOD is by improving the relative frequency stability, that is, by reducing the relative short-term frequency fluctuation $\sigma_{\min}$. Because the (short-term) frequency stability is closely linked to the quality factor of the resonance, the designer should select a resonator geometry (and mode shape) that maximizes Q and, thus, minimizes $\sigma_{\min}$ (i.e., reduces the relative amount of frequency noise, thereby improving the frequency stability). This is the main motivation for exploring more complex beam structures, such as the hammerhead resonators presented in this work. As mentioned before, Q and G_R cannot generally be optimized independently, and changes to the layer structure of the beam will likely affect Q.

Because resonant chemical sensors operate under ambient conditions, either in air or in liquid, the fluid damping is often the dominating damping mechanism. Assuming that the beam's vibration mode shape in the fluid can be approximated by that in vacuum, and assuming a harmonic tip force as the

excitation force, Heinrich et al.(32) have derived a simple equation for the quality factor of prismatic beams vibrating in the fundamental IP resonance mode

$$Q_{\mathrm{fluid}} \approx 0.7124 \left[\frac{E_{\mathrm{eff}}{\rho_{\mathrm{eff}}}^3}{\eta^2 \rho_{\mathrm{f}}^2}\right]^{1/4} \frac{h\sqrt{b}}{L} \quad (10)$$

Here, η and ρ_{f} denote the viscosity and density of the fluid, respectively. Equation 10 was derived under the assumption that the fluid interacts with the cantilever only on the cantilever surfaces that are shearing the fluid and indicates that Q increases proportional to $b^{1/2}/L$, that is, proportionally to the square root of the IP resonance frequency for fixed values of the effective modulus and effective density (see eq 5). Moreover, Q increases with increasing beam thickness *h* because of the increased beam inertia. Again, eq 10 represents the Q because of fluid damping only. For cantilevers operated in liquid (water), this is by far the dominant damping mechanism and the measured Q -factor for prismatic beams operated in water follows the geometric dependencies highlighted in eq 10 over a wide range of frequencies and cantilever thicknesses, as is highlighted in the Supporting Information, Figure S4.(23,32) If operated in air, other loss mechanisms, such as the anchor or support loss, must be considered as well. Hao et al.(33) developed an analytical model for the Q factor due to support loss for prismatic cantilevers vibrating in their IP vibration mode, with the resulting Q due to anchor loss being proportional to the cube of the length to width ratio

$$Q_{\mathrm{anchor}} = \left[\frac{0.24(1-\nu)}{(1+\nu)\Psi}\right] \frac{1}{(\beta_n \chi_n)^2} \left[\frac{L}{b}\right]^3 \quad (11)$$

Here, ν is the Poisson ratio, ψ is a loss term (see ref (33) for details), β_n is the mode constant, and χ_n is the mode shape factor. Equation 11 indicates that especially for short and wide cantilevers, the anchor loss may become dominant. This seems to be confirmed by the experimental data shown in Figure 6, displaying the measured Q -factor of the fundamental IP resonance mode as a function of the square root of the resonance frequency for 45 µm wide prismatic cantilevers with length ranging from 200 to 1000 µm and silicon thickness from 5 to 20 µm (with an added 2 µm passivation). Within this parameter range, the Q -factor seems to follow the geometrical dependence described by eq 10 for the longer cantilever beams ($L \geq 400$ µm). For the shortest beams with a length of 200 µm, corresponding to the highest resonance frequencies, a deviation from the geometrical dependencies of eq 10 is noted especially for the thickest cantilevers, likely because of support loss stemming from the resulting small (L/b) ratio and the impact of the neglected fluid effects on the smaller faces of the cantilever. However, more data on shorter and/or thicker cantilevers would be needed to confirm this. Among the cantilever lengths tested, those with a length of 400 µm often exhibited the highest Q -factor and, thus, offer a good compromise between being dominated either by support loss or air/liquid damping.

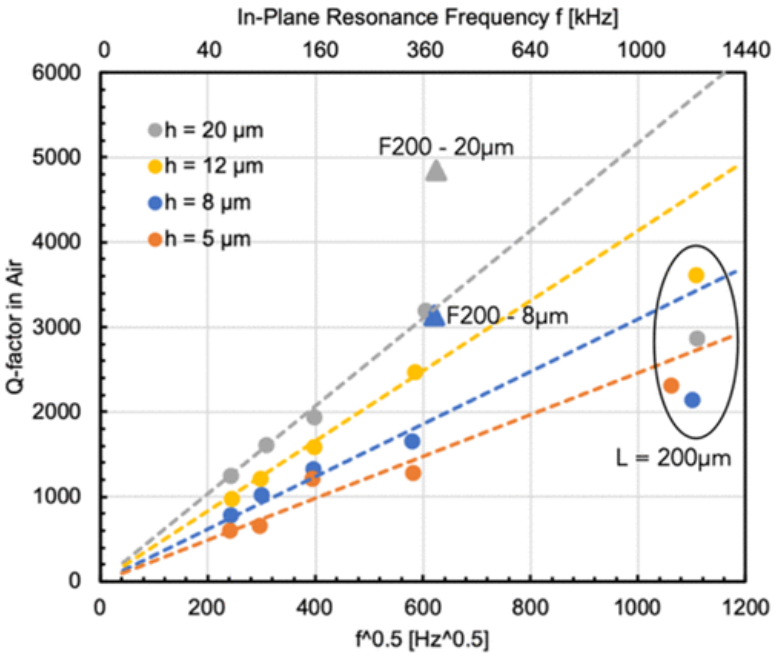

Figure 6. Measured Q -factor in air of the fundamental IP resonance mode as a function of the square root of the resonance frequency for 45 µm wide prismatic cantilevers with lengths of 200, 400, 600, 800, and 1000 µm and silicon thicknesses of 5, 8, 12, and 20 µm; the dashed lines represent linear fits through data points except *L* = 200 µm of a respective thickness. The triangles represent Q -factor and resonance frequency of two F200B hammerhead resonators with 200 µm outer radius and a 45 µm wide and 100 µm long stem, one with 8 µm, the other with 20 µm silicon thickness. All resonators have an approximately 2 µm passivation on top.

One of the key observations and motivations for this work is that the Q-factors of hammerhead resonators vibrating in their fundamental IP mode are consistently higher than those of their prismatic beam counterparts with similar IP resonance frequency and thickness. To illustrate this, Figure 6 also shows the measured Q -factor for two hammerhead resonators with 200 µm outer radius (F200B), one with 8 µm and the other with 20 µm silicon thickness. The difference in Q is distinct and well beyond the device-to-device variation of the measured Q -factors. For example, a 45 µm-wide and 400 µm-long prismatic beam with a silicon thickness of 20 µm experiences a measured Q -factor of 3200 at an IP resonance frequency of 365 kHz, while a hammerhead resonator with a 45 µm-wide and 100 µm-long stem region and a semiannular head region with 200 µm outer diameter and the same device thickness shows a 50% increased measured Q -factor of 4850 at a frequency of 390 kHz, both in air. This increase in Q -factor translates into better frequency stability and, ultimately, improved sensor LOD. More data supporting this are shown in the Supporting Information, Table S1.

A possible explanation for this increased Q -factor hinges on the fact that the semicircular head of the hammerhead structure increases the effective mass of the resonator over that of a prismatic beam and that this larger effective mass increases the quality factor. If one considers a simple linear oscillator with mass *m*, spring constant *k*, and damping coefficient *c*, the quality factor can be written as

$$Q = \frac{2\sqrt{km}}{c} \quad (12)$$

One can now apply eq 12 separately to the prismatic beam resonator (#1) and hammerhead resonator (#2). If one assumes that (i) the hammerhead resonator has a larger (effective) mass m_2 =

$\alpha \times m_1$ with $\alpha > 1$ and (ii) the resonance frequencies of both structures are the same, that is, $k_1/m_1 = k_2/m_2$, the ratio of the Q -factors can be easily derived as

$$\frac{Q_2}{Q_1} = \alpha \frac{c_1}{c_2} \quad (13)$$

Equation 13 indicates that the larger effective mass of the hammerhead resonator tends to increase its Q -factor compared to that of the prismatic beam with the same resonance frequency. However, what is the role of the factor c_1/c_2, the ratio of the damping coefficients? One can envision certain aspects of the hammerhead device that tend to decrease the losses. For example, the semicircular head translates and also rotates, and this rotation is expected to be very efficient with respect to the interaction with the surrounding fluid. A drawback for the hammerhead device is that the cantilever "stem" is necessarily stiffer (shorter and/or wider) to give the same natural frequency as the pure cantilever, which is expected to increase support losses. The sensor's LOD given in eq 1 is particularly affected by this geometrical dependence of Q in that $\Delta f_{\min}$ is generally improved (i.e., reduced) by increasing the quality factor of the resonance, which is the primary motivation behind investigating IP rather than OOP cantilever modes. In addition, utilizing the IP mode (in comparison to the fundamental OOP mode) results in lower mass-loading because of the surrounding fluid, which helps to reduce the cantilever's starting mass and thus improve its gravimetric sensitivity.

Furthermore, hammerhead devices exhibit decoupling of the section of the cantilever where most of the deformation occurs from the portion where mass is loaded onto the device, resulting in an opportunity to replace a portion of the hammerhead with polymer (or another material), which can absorb the analyte. This has been investigated by creating "bathtub" structures where a portion of the semicircular annulus of the hammerhead is etched leaving an area that can then be backfilled with material to absorb analyte.(34) Such a structure (see the Supporting Information, Figure S5) can aid in creating a more uniform polymer film and also creates an area to contain the polymer (or other analyte-sensitive material) so that it does not flow into the portion of the beam where bending dominates. It should be mentioned though that in the case of a "bathtub" structure, the layer sandwich is no longer uniform, and thus, eqs 8 and 9 are no longer valid. Thus, bathtub structures were not used in this work. However, for the hammerheads tested here, the sensing film has been deposited on the head regions only. Many of the sensitive films used in gas sensing have viscoelastic properties that dampen the beam's vibration, thus isolating this film from the portion of the beam where most of the bending occurs during resonance is beneficial in terms of reducing any potential unwanted energy losses.

Hammerhead Resonator Testing

The amplitude and phase-transfer characteristics of the uncoated hammerhead resonators were measured both electrically at the output of the piezoresistive Wheatstone bridge and optically by looking at the device vibration using a Polytec MSA-500 Micro System Analyzer (Polytec, Waldbronn, Germany). For characterization, the hammerhead dice were wire-bonded to dual in-line (DIL) packages. The electrical, open-loop transfer characteristics of the hammerhead resonators were measured using a network analyzer (Agilent 4395A, Santa Clara, CA) and a circuit fabricated on a custom-printed circuit board (PCB) was used to interface the resonators with the network analyzer. The excited and detected mode shapes were identified by comparing measured and simulated resonance frequencies and by

measuring the actual mode shapes using the Polytec vibrometer. Figure 7 presents sample results for both optical and electrical characterizations of F200B resonators with an outer radius of 200 µm and a 20 µm silicon thickness. The corresponding simulated mode shapes are superimposed as well as the Q -factors extracted from the optical measurements. Clearly, the fundamental IP resonance frequency is well separated from nearby frequencies of other modes, which simplifies operation of the resonator in closed loop. Moreover, the fundamental IP resonance frequency exhibits the highest Q -factor in air with $Q \approx 4800$ compared to the OOP and torsional modes in the tested frequency range. Figure 7b highlights the efficiency of the U-shaped Wheatstone bridge in promoting signals stemming from the IP mode, with the signals of the fundamental OOP and torsional modes being at least 15 dB smaller. Furthermore, the optical and electrical transfer characteristics around the fundamental IP mode show the expected −180° phase shift across the resonance (see the Supporting Information, Figure S6); however, the phase at resonance is not −90°, which can be explained by electrical cross-talk in the case of the purely electrical measurements. A proper phase adjustment is thus typically required for closed-loop operation.

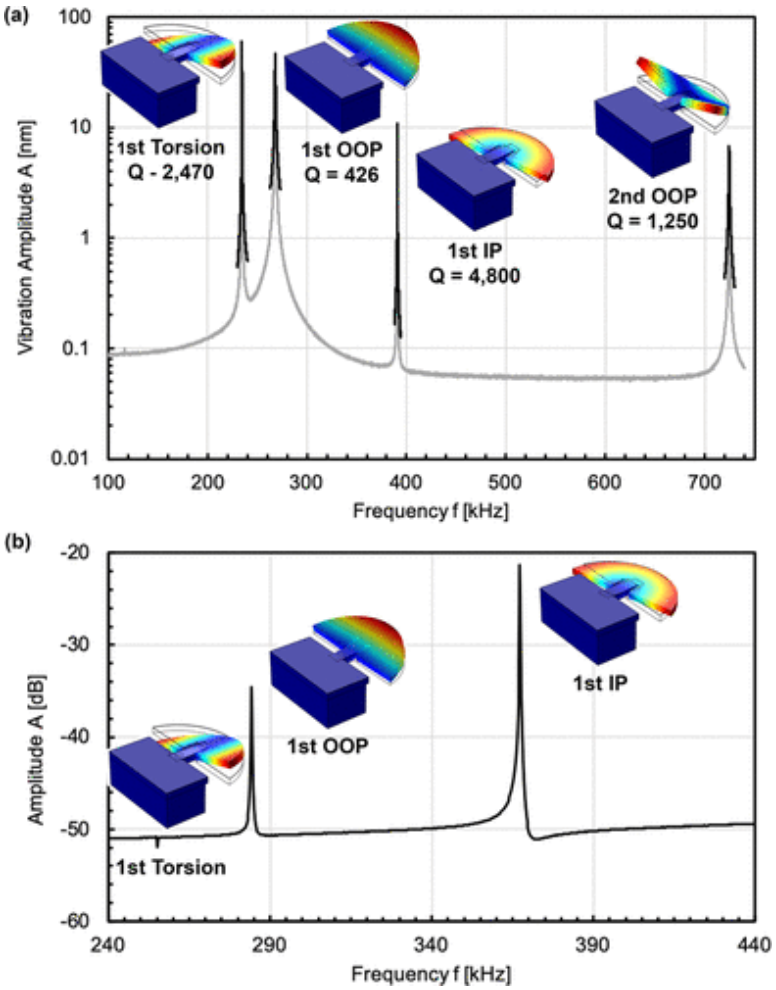

Figure 7. (a) OOP vibration amplitude—measured using Polytec MSA-500—of F200B resonator with 20 µm silicon thickness excited with $V_{\mathrm{dc}} = 1$ V and $V_{\mathrm{ac}} = 1\ V_{\mathrm{p}}$ as a function of frequency with four vibration modes between 100 and 750 kHz identified by finite-element simulation; the solid black lines represent detailed measurements around the individual resonance frequencies and (b) piezoresistive amplitude-transfer characteristic of F200B resonator with 20 µm silicon thickness as a function of frequency.

As mentioned in the motivation for this work, the Q -factor of the fundamental IP resonance mode of the hammerhead resonators was consistently larger than that of prismatic cantilevers with comparable IP resonance frequencies. This is further highlighted in the Supporting Information, Table S1, which compares measured Q -factors of the fundamental IP resonance modes of select hammerhead and prismatic beam resonators with 8 and 20 μm silicon thicknesses, respectively. The resonators considered in the table were not coated with any polymeric sensing film.

Gas-Phase Chemical Testing

For gas-phase testing, the hammerhead resonators were spray-coated with chemically sensitive polymer films using a commercial spray gun. A shadow mask was used to cover parts of the resonator that should not be coated with the polymer. In the case of hammerhead resonators, only the head region is coated to minimize the Q -factor degradation that would arise because of coating of the stem region.

For closed-loop operation, the cantilevers are placed in an amplifying feedback loop, which has been previously described.(17) The signal from the amplifying feedback loop is then fed into a benchtop frequency counter. The frequency counter interfaces with LabVIEW (National Instruments, Austin, TX) and a LabVIEW program is used to store the frequency data to a text file for analysis. Gas-phase sensing experiments are performed using a custom-constructed gas setup previously described.(17) The gas setup is controlled using LabVIEW. Nitrogen used as a carrier gas is flowed through temperature-controlled bubblers containing the analyte of interest. To adjust the analyte concentration, the stream of gas from the bubbler is further diluted by combining it with a stream of pure nitrogen. The total flow rate is kept constant at 80 mL/min. The analyte is then flowed into a custom-machined chamber containing the cantilever die. The PCB board for the closed-loop operation attaches to the bottom of the DIL package via a zero insertion force socket.

Figure 8 shows a characteristic closed-loop measurement, that is, the measured frequency change as a function of time, for a F200A resonator with 20 μm silicon thickness coated with a 1.5 μm poly(isobutylene) (PIB) sensing film exposed to different toluene concentrations. The coated device in the measurement chamber is exposed to the analyte for 5 min, followed by a flushing with the carrier gas. As expected, the resonance frequency decreases upon analyte exposure and then recovers when pure nitrogen is flowed through the setup. Similar measurements for benzene and *m*-xylene are shown in the Supporting Information, Figure S7.

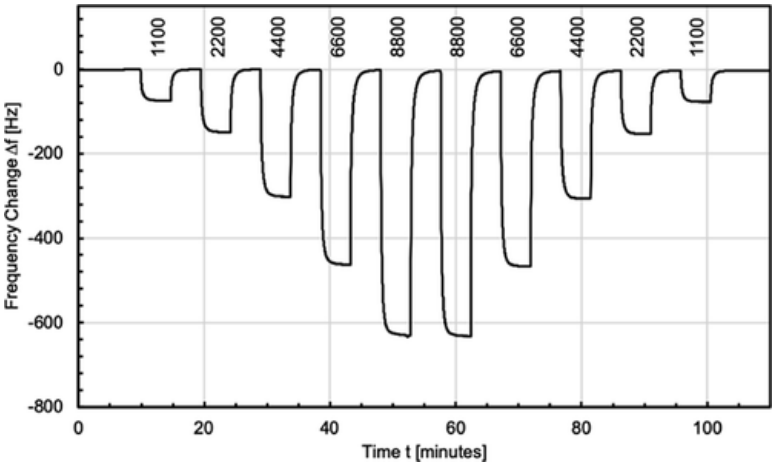

Figure 8. Sample gas measurement exposing a F200A hammerhead resonator (20 µm silicon thickness) coated with 1.5 µm PIB to different toluene concentrations. Analyte concentrations in ppm are shown in the graph.

As discussed earlier, the short-term frequency stability dictates the smallest change in frequency that can be resolved. The frequency stabilities measured for polymer-coated hammerhead resonators are typically on the order of 5–30 mHz. For the F200A resonator coated with 1.5 µm PIB (see the measurement data shown in Figure 8), a frequency stability of 28.5 mHz, corresponding to an Allan variance of 7.7×10^{-8}, has been extracted.

Using the data from Figure 8 and similar measurements done with the same resonator for other analytes (Supporting Information, Figure S7), Figure 9 plots the extracted absolute values of the measured steady-state frequency changes for the coated F200A hammerhead resonator exposed to the three different aromatic compounds as a function of the analyte concentrations. In the tested concentration range, the sensor response is linear and measurements at increasing and decreasing analyte concentrations show minimal sensor hysteresis. The sensor sensitivities in Hz/ppm obtained by linear regression are shown in Figure 9.

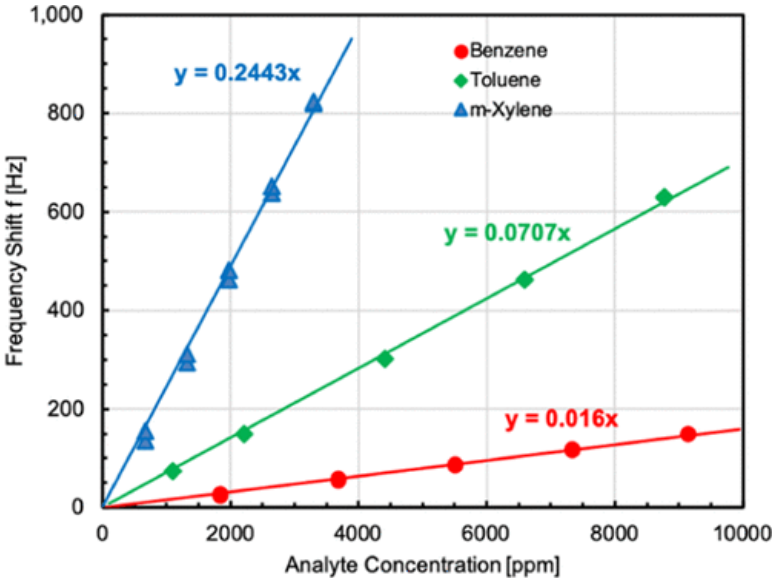

Figure 9. Sensitivity curves showing the absolute value of the measured steady-state frequency change for the F200A hammerhead resonator coated with 1.5 µm PIB as a function of *m*-xylene, toluene, and benzene concentrations.

To consider the thermodynamics of analyte sorption into the sensing film, the data presented have been normalized in the following way (Supporting Information, Figure S8): as *y*-axis, the frequency change divided by the analyte molecular weight is displayed, which is proportional to the number of absorbed analyte molecules rather than the absorbed mass; as *x*-axis, the analyte concentration is normalized by the saturated analyte concentration at room temperature, thus displaying the % of saturated vapor pressure. When normalized, the sensitivity curves for the three analytes almost coincide, meaning that PIB itself has less inherent selectivity for the three aromatic hydrocarbons.

Finally, Table1 summarizes the measured frequency stability, sensor sensitivity to the three analytes, and extrapolated LOD (using eq 1) for the 20 µm-thick F200A resonator coated with a 1.5 µm PIB sensing film based on the data presented in Figure 9. For the case of *m*-xylene, the PIB-coated F200A device enables sub-500-ppb detection limits without any preconcentration. Several F150A resonators coated with a PIB sensing films have also been tested using toluene as an analyte, with the results being summarized in Table1 as well. Extrapolated LODs for toluene are in the range of 500–1000 ppb. It is interesting to see the impact of the sensing film thickness and silicon thickness on the results: for F150A resonators with 20 µm Si thickness, the increase in sensing film thickness (from 1.5 to 3 µm) results—as expected from eq 9—in a higher sensitivity at the expense of a reduced frequency stability, likely because of the increased losses from the added viscoelastic sensing film; reducing the Si thickness (from 20 to 8 µm) while keeping the PIB thickness the same increases—as expected from eq 9—the sensitivity but again at the expense of a reduced frequency stability because of the decreased inertia. Ultimately, in this case, the thicker resonator coated with the thicker sensing film yields the lowest LOD.

Table 1. Summary of Performance Data of Tested Hammerhead and Cantilever Devices with Extrapolated LOD for Different Analytes

device and coating	resonance frequency f_{ip} [kHz]	freq. stability Δf_{min} [Hz]	analyte	sensitivity [Hz/ppm]	extrapolated LOD [ppb]
F200A, 20 µm Si, 1.5 µm PIB	**368.5**	**0.0285**	**benzene**	**0.016**	**5300**
			toluene	**0.071**	**1200**
			***m*-xylene**	**0.244**	**350**
F150A, 20 µm Si, 1.5 µm PIB	**804.2**	**0.0048**	**toluene**	**0.016**	**910**
F150A, 20 µm Si, 3 µm PIB	**851.9**	**0.0058**	**toluene**	**0.032**	**550**
F150A, 8 µm Si, 3 µm PIB	**803.7**	**0.0128**	**toluene**	**0.054**	**710**
45W200L, 20 µm Si, 3 µm PIB	**1248.2**	**0.0355**	**toluene**	**0.051**	**2090**

Table1 also shows a comparison of the hammerhead sensor data with a 200 µm-long and 45 µm-wide prismatic cantilever with 20 µm Si thickness. For a 3 µm PIB coating, the 45W200L cantilever yields a higher sensitivity (because of the higher f_{ip}) compared to the 20 µm F150A with the same sensing film thickness, but the inferior frequency stability (0.0355 vs 0.0058 Hz) of the prismatic cantilever reduces the LOD to 2 ppm. This highlights the advantage of the hammerhead resonators compared to simple prismatic cantilevers.

Conclusions

This work demonstrates the potential of IP hammerhead resonators, comprising a semicircular annulus supported by a cantilever stem and vibrating in the fundamental IP resonance mode, as chemical sensing platforms for gas-phase chemical sensor applications. The hammerhead resonators have been shown to deliver higher sensing performance compared to IP cantilevers with similar resonance frequencies. This improvement is primarily driven by the higher quality factors observed by the hammerhead resonators, again as compared to cantilevers with similar layer sandwich and IP resonance frequencies. It is believed that the higher effective mass of the hammerhead resonators due to the shape of the head yields an increased kinetic energy, which benefits the Q -factor. This higher Q -factor translates into improved short-term frequency stability, which yields better LOD. It is interesting to see that thicker resonators appear to result in improved LOD over thinner devices. The improved frequency stability—which also seems less affected by thicker sensing films—that results from operating a thicker hammerhead appears to make up for the reduction in gravimetric sensitivity caused by the higher starting mass. This has practical implications as thicker resonators are generally more sturdy and easier to fabricate. Last, the head region of the hammerhead resonators facilitates localized sensing film deposition, where not coating the stem region reduces the adverse effects that the viscoelastic polymer film has on the Q -factor of the resonator.

While the hammerhead resonator platform improves the resonator sensitivity and LOD compared to simple cantilever structures, the sensor stability and selectivity still require attention. Thermal drift, due to the high temperature coefficient of frequency for silicon, leads to frequency changes that will add to the device noise.(35,36) Differential measurements using an uncoated reference sensor can address this. Similarly, changes that occur over time in the chemically sensitive films are another example of an effect that can alter the sensor signal over time. In addition, the polymer films used in this investigation only show partial selectivity to volatile organic compounds. Actual applications such as air-quality monitoring will require greater selectivity among volatile organic compounds, as can be, for example, achieved by coating several sensors of an array using different sensing films.(37)

Supporting Information

The Supporting Information is available free of charge at https://pubs.acs.org/doi/10.1021/acssensors.9b01651.

- Details on sensor design and fabrication, including excitation and sensing resistor layout and schematic of the fabrication process; schematic of a prismatic cantilever; measured Q -factors in water of IP prismatic cantilevers; SEM image of bathtub hammerhead device; optical and piezoresistive transfer characteristic of hammerhead resonator around fundamental IP resonance; sample gas measurement exposing PIB-coated hammerhead resonator to benzene and *m*-xylene; normalized sensitivity curves for toluene, benzene, and *m*-xylene; and comparison of Q -factors and resonance frequencies of prismatic cantilevers and hammerhead resonators (PDF)

pdf

se9b01651_si_001.pdf (920.0 kb)

Notes

Neither the Department of the Navy nor any other component of the Department of Defense has approved, endorsed, or authorized this product.

Terms & Conditions

Acknowledgments

This work was performed in part at the Georgia Tech Institute for Electronics and Nanotechnology, a member of the National Nanotechnology Coordinated Infrastructure (NNCI), which is supported by the National Science Foundation (ECCS-1542174). The authors would like to thank the staff of the Institute for Electronics and Nanotechnology for their support during device fabrication. This research was also funded in part by the National Science Foundation under awards EECS-0824017, ECCS-1128554, and ECCS-1128992.

References

1 Kassal, P.; Steinberg, M. D.; Steinberg, I. M. Wireless Chemical Sensors and Biosensors: A Review. *Sens. Actuators, B* **2018**, *266*, 228– 245, DOI: 10.1016/j.snb.2018.03.074

2 Hierlemann, A. CMOS-based Chemical Sensors. *CMOS-MEMS*; Advanced Micro and Nanosystems; Wiley, **2008**; pp 335– 390.

3 Hierlemann, A.; Brand, O.; Hagleitner, C.; Baltes, H. Microfabrication Techniques for Chemical/biosensors. *Proc. IEEE* **2003**, *91*, 839– 863, DOI: 10.1109/jproc.2003.813583

4 Bandodkar, A. J.; Wang, J. Non-Invasive Wearable Electrochemical Sensors: A Review. *Trends Biotechnol.* **2014**, *32*, 363– 371, DOI: 10.1016/j.tibtech.2014.04.005

5 Hierlemann, A.; Baltes, H. CMOS-Based Chemical Microsensors. *Analyst* **2003**, *128*, 15– 28, DOI: 10.1039/b208563c

6 Anichini, C.; Czepa, W.; Pakulski, D.; Aliprandi, A.; Ciesielski, A.; Samorì, P. Chemical Sensing with 2D Materials. *Chem. Soc. Rev.* **2018**, *47*, 4860– 4908, DOI: 10.1039/c8cs00417j

7 Beardslee, L. A.; Brand, O.; Josse, F. Chemical Sensors. *Resonant MEMS*; Advanced Micro- and Nanosystems; Wiley-VCH, **2015**; pp 355– 391.

8 Johnson, B. N.; Mutharasan, R. Biosensing Using Dynamic-Mode Cantilever Sensors: A Review. *Biosens. Bioelectron.* **2012**, *32*, 1– 18, DOI: 10.1016/j.bios.2011.10.054

9 Waggoner, P. S.; Craighead, H. G. Micro- and Nanomechanical Sensors for Environmental, Chemical, and Biological Detection. *Lab Chip* **2007**, *7*, 1238– 1255, DOI: 10.1039/b707401h

10 Datar, R.; Kim, S.; Jeon, S.; Hesketh, P.; Manalis, S.; Boisen, A.; Thundat, T. Cantilever Sensors: Nanomechanical Tools for Diagnostics. *MRS Bull.* **2009**, *34*, 449– 454, DOI: 10.1557/mrs2009.121

11 Eom, K.; Park, H. S.; Yoon, D. S.; Kwon, T. Nanomechanical Resonators and Their Applications in Biological/chemical Detection: Nanomechanics Principles. *Phys. Rep.* **2011**, *503*, 115– 163, DOI: 10.1016/j.physrep.2011.03.002

12 Boisen, A.; Dohn, S.; Keller, S. S.; Schmid, S.; Tenje, M. Cantilever-like Micromechanical Sensors. *Rep. Prog. Phys.* **2011**, *74*, 036101, DOI: 10.1088/0034-4885/74/3/036101

13 Lavrik, N. V.; Sepaniak, M. J.; Datskos, P. G. Cantilever Transducers as a Platform for Chemical and Biological Sensors. *Rev. Sci. Instrum.* **2004**, *75*, 2229– 2253, DOI: 10.1063/1.1763252

14 Devkota, J.; Ohodnicki, P.; Greve, D. SAW Sensors for Chemical Vapors and Gases. *Sensors* **2017**, *17*, 801, DOI: 10.3390/s17040801

15 Ballantine, D. S.; White, R. M.; Martin, S. J.; Ricco, A. J.; Zellers, E. T.; Frye, G. C.; Wohltjen, H.; Levy, M.; Stern, R. *Acoustic Wave Sensors: Theory, Design and Physico-Chemical Applications*; Applications of Modern Acoustics; Elsevier Science, **1996**.

16 Panneerselvam, G.; Thirumal, V.; Pandya, H. M. Review of Surface Acoustic Wave Sensors for the Detection and Identification of Toxic Environmental Gases/Vapours. *Arch. Acoust.* **2018**, *43*, 357– 367, DOI: 10.24425/123908

17 Demirci, K. S.; Beardslee, L. A.; Truax, S.; Su, J.-J.; Brand, O. Integrated Silicon-Based Chemical Microsystem for Portable Sensing Applications. *Sens. Actuators, B* **2013**, *180*, 50– 59, DOI: 10.1016/j.snb.2012.01.061

18 Bausells, J. Piezoresistive cantilevers for nanomechanical sensing. *Microelectron. Eng.* **2015**, *145*, 9– 20, DOI: 10.1016/j.mee.2015.02.010

19 Mathew, R.; Ravi Sankar, A. A Review on Surface Stress-Based Miniaturized Piezoresistive SU-8 Polymeric Cantilever Sensors. *Nano-Micro Lett.* **2018**, *10*, 35, DOI: 10.1007/s40820-018-0189-1

20 Wu, H.; Sang, L.; Li, Y.; Teraji, T.; Li, T.; Imura, M.; You, J.; Koide, Y.; Toda, M.; Liao, M. Reducing Intrinsic Energy Dissipation in Diamond-on-Diamond Mechanical Resonators toward One Million Quality Factor. *Phys. Rev. Mater.* **2018**, *2*, 090601(R) DOI: 10.1103/physrevmaterials.2.090601

21 Possas-Abreu, M.; Ghassemi, F.; Rousseau, L.; Scorsone, E.; Descours, E.; Lissorgues, G. Development of Diamond and Silicon MEMS Sensor Arrays with Integrated Readout for Vapor Detection. *Sensors* **2017**, *17*, 1163, DOI: 10.3390/s17061163

22 Beardslee, L. A.; Demirci, K. S.; Luzinova, Y.; Mizaikoff, B.; Heinrich, S. M.; Josse, F.; Brand, O. Liquid-Phase Chemical Sensing Using Lateral Mode Resonant Cantilevers. *Anal. Chem.* **2010**, *82*, 7542– 7549, DOI: 10.1021/ac1010102

23 Beardslee, L. A.; Josse, F.; Heinrich, S. M.; Dufour, I.; Brand, O. Geometrical considerations for the design of liquid-phase biochemical sensors using a cantilever's fundamental in-plane mode. *Sens. Actuators, B* **2012**, *164*, 7– 14, DOI: 10.1016/j.snb.2012.01.035

24 Beardslee, L. A.; Addous, A. M.; Heinrich, S.; Josse, F.; Dufour, I.; Brand, O. Thermal Excitation and Piezoresistive Detection of Cantilever In-Plane Resonance Modes for Sensing Applications. *J. Microelectromech. Syst.* **2010**, *19*, 1015– 1017, DOI: 10.1109/jmems.2010.2052093

25 Dufour, I.; Lemaire, E.; Caillard, B.; Debéda, H.; Lucat, C.; Heinrich, S. M.; Josse, F.; Brand, O. Effect of Hydrodynamic Force on Microcantilever Vibrations: Applications to Liquid-Phase Chemical Sensing. *Sens. Actuators, B* **2014**, *192*, 664– 672, DOI: 10.1016/j.snb.2013.10.106

26 Beardslee, L. A. Liquid-Phase Operation of MEMS Resonators for Biochemical Sensing in Point of Care and Embedded Applications. Ph.D. Thesis; Georgia Institute of Technology, **2011**.

27 Allan, D. W.; Barnes, J. A. A Modified "Allan Variance" with Increased Oscillator Characterization Ability. *Thirty Fifth Annual Frequency Control Symposium*, **1981**; pp 470– 475.

28 Lange, D.; Hagleitner, C.; Hierlemann, A.; Brand, O.; Baltes, H. Complementary Metal Oxide Semiconductor Cantilever Arrays on a Single Chip: Mass-Sensitive Detection of Volatile Organic Compounds. *Anal. Chem.* **2002**, *74*, 3084– 3095, DOI: 10.1021/ac011269j

29 Heinrich, S. M.; Dufour, I. Fundamental Theory of Resonant MEMS Devices. *Resonant MEMS*; Advanced Micro- and Nanosystems; Wiley-VCH, **2015**; pp 3– 28.

30 Vančura, C.; Lichtenberg, J.; Hierlemann, A.; Josse, F. Characterization of Magnetically Actuated Resonant Cantilevers in Viscous Fluids. *Appl. Phys. Lett.* **2005**, *87*, 162510, DOI: 10.1063/1.2108130

31 Ayela, C.; Dubourg, G.; Pellet, C.; Haupt, K. All-Organic Microelectromechanical Systems Integrating Specific Molecular Recognition - A New Generation of Chemical Sensors. *Adv. Mater.* **2014**, *26*, 5876– 5879, DOI: 10.1002/adma.201401088

32 Heinrich, S.; Maharjan, R.; Dufour, I.; Josse, F.; Beardslee, L.; Brand, O. An Analytical Model of a Thermally Excited Microcantilever Vibrating Laterally in a Viscous Fluid. *IEEE Sensors*; IEEE, **2010**; pp 1399– 1404.

33 Hao, Z.; Erbil, A.; Ayazi, F. An Analytical Model for Support Loss in Micromachined Beam Resonators with in-Plane Flexural Vibrations. *Sens. Actuators, A* **2003**, *109*, 156– 164, DOI: 10.1016/j.sna.2003.09.037

34 Carron, C.; Getz, P.; Su, J.; Gottfried, D. S.; Brand, O.; Josse, F.; Heinrich, S. M. Cantilever-Based Resonant Gas Sensors with Integrated Recesses for Localized Sensing Layer Deposition. *IEEE Sensors*; IEEE, **2013**; pp 1– 4.

35 Samarao, A. K.; Ayazi, F. Temperature Compensation of Silicon Resonators via Degenerate Doping. *IEEE Trans. Electron Devices* **2012**, *59*, 87– 93, DOI: 10.1109/ted.2011.2172613

36 Thakar, V. A.; Wu, Z.; Peczalski, A.; Rais-Zadeh, M. Piezoelectrically Transduced Temperature-Compensated Flexural-Mode Silicon Resonators. *J. Microelectromech. Syst.* **2013**, *22*, 815– 823, DOI: 10.1109/jmems.2013.2245403

37 Hierlemann, A.; Gutierrez-Osuna, R. Higher-Order Chemical Sensing. *Chem. Rev.* **2008**, *108*, 563– 613, DOI: 10.1021/cr068116m